(2)

OFFICE OF NAVAL RESEARCH

Contract N00014-82K-0612

Task No. NR 627-838

TECHNICAL REPORT NO. 62

# Molecular and Supermolecular Origins of Enhanced Electronic Conductivity in Template-Synthesized Polyheterocyclic Fibrils Part I. Supermolecular Effects

by

Zhihua Cai, Junting Lei, Wenbin Liang and Charles R. Martin

Department of Chemistry
Colorado State University
Ft. Collins, CO 80523

Prepared for publication

in

Chemistry of Materials

July 18, 1991

# REPORT DOCUMENTATION PAGE

Form Approved
OMB No. 0704-0188

| | |
|---|---|
| 1a. REPORT SECURITY CLASSIFICATION<br>UNCLASSIFIED | 1b. RESTRICTIVE MARKINGS |
| 2a. SECURITY CLASSIFICATION AUTHORITY | 3. DISTRIBUTION/AVAILABILITY OF REPORT<br>APPROVED FOR PUBLIC DISTRIBUTION, DISTRIBUTION UNLIMITED. |
| 2b. DECLASSIFICATION/DOWNGRADING SCHEDULE | |
| 4. PERFORMING ORGANIZATION REPORT NUMBER(S)<br>ONR TECHNICAL REPORT 62 | 5. MONITORING ORGANIZATION REPORT NUMBER(S) |
| 6a. NAME OF PERFORMING ORGANIZATION<br>Dr. Charles R. Martin<br>Department of Chemistry<br>6b. OFFICE SYMBOL (If applicable) | 7a. NAME OF MONITORING ORGANIZATION<br>Office of Naval Research |
| 6c. ADDRESS (City, State, and ZIP Code)<br>Colorado State University<br>Ft. Collins, CO 80523 | 7b. ADDRESS (City, State, and ZIP Code)<br>800 North Quincy Street<br>Arlington, VA 22217 |
| 8a. NAME OF FUNDING/SPONSORING ORGANIZATION<br>Office of Naval Research<br>8b. OFFICE SYMBOL (If applicable) | 9. PROCUREMENT INSTRUMENT IDENTIFICATION NUMBER<br>Contract # N00014-82K-0612 |
| 8c. ADDRESS (City, State, and ZIP Code)<br>800 North Quincy Street<br>Arlington, VA 22217 | 10. SOURCE OF FUNDING NUMBERS<br>PROGRAM ELEMENT NO. / PROJECT NO. / TASK NO / WORK UNIT ACCESSION NO |
| 11. TITLE (Include Security Classification)<br>Molecular and Supermolecular Origins of Enhanced Electronic Conductivity in Template-Synthesized Polyheterocyclic Fibrils. Part I. Supermolecular Effects | |
| 12. PERSONAL AUTHOR(S)<br>Zhihua Cai, Junting Lei, Wenbin Liang and Charles R. Martin | |
| 13a. TYPE OF REPORT<br>Technical<br>13b. TIME COVERED<br>FROM _____ TO _____ | 14. DATE OF REPORT (Year, Month, Day)<br>(91,7,18) July 18, 1991<br>15. PAGE COUNT |
| 16. SUPPLEMENTARY NOTATION | |

| 17 COSATI CODES | | |
|---|---|---|
| FIELD | GROUP | SUB-GROUP |
| | | |
| | | |

18. SUBJECT TERMS (Continue on reverse if necessary and identify by block number)
Electronically conductive polymers, polypyrrole, synthetic metals


19. ABSTRACT (Continue on reverse if necessary and identify by block number)

The pores in a nanoporous membrane can be used as templates for the synthesis of nanostructures. We have recently shown that conductive polymer fibrils, obtained via this "template" synthetic method, can show dramatically higher electronic conductivities than conventional versions of the analogous polymers. In this and a succeeding paper we explore the molecular and supermolecular origins of this enhanced electronic conductivity. This paper focuses on supermolecular effects. We have used DC and optical measurements of conductivity, x-ray diffraction, and polarized infrared absorption spectroscopy to show that the polymer chains in the narrowest template-synthesized fibrils are preferentially oriented parallel to the axes of these fibrils. This preferential polymer chain orientation is partially responsible for the observed conductivity enhancements. We also show that template-synthesis can yield poly(3-methylthiophene) fibrils with conductivities as high as 6600 S $cm^{-1}$. This is the highest conductivity ever reported for a heterocyclic polymer.


| | |
|---|---|
| 20. DISTRIBUTION/AVAILABILITY OF ABSTRACT<br>☒ UNCLASSIFIED/UNLIMITED ☐ SAME AS RPT ☐ DTIC USERS | 21. ABSTRACT SECURITY CLASSIFICATION<br>UNCLASSIFIED |
| 22a. NAME OF RESPONSIBLE INDIVIDUAL<br>Dr. Robert Nowak | 22b TELEPHONE (Include Area Code)<br>(202) 696-4410<br>22c. OFFICE SYMBOL |

DD Form 1473, JUN 86 *Previous editions are obsolete.* SECURITY CLASSIFICATION OF THIS PAGE

# MOLECULAR AND SUPERMOLECULAR ORIGINS OF ENHANCED ELECTRONIC CONDUCTIVITY IN TEMPLATE-SYNTHESIZED POLYHETEROCYCLIC FIBRILS

## PART I. SUPERMOLECULAR EFFECTS

Zhihua Cai, Junting Lei, Wenbin Liang, and Charles R. Martin*

Department of Chemistry

Colorado State University

Fort Collins, CO 80523

Corresponding author.

A-1

## ABSTRACT

The pores in a nanoporous membrane can be used as templates for the synthesis of nanostructures. We have recently shown that conductive polymer fibrils, obtained via this "template" synthetic method, can show dramatically higher electronic conductivities than conventional versions of the analogous polymers. In this and a succeeding paper we explore the molecular and supermolecular origins of this enhanced electronic conductivity. This paper focuses on supermolecular effects. We have used DC and optical measurements of conductivity, X-ray diffraction, and polarized infrared absorption spectroscopy to show that the polymer chains in the narrowest template-synthesized fibrils are preferentially oriented parallel to the axes of these fibrils. This preferential polymer chain orientation is partially responsible for the observed conductivity enhancements. We also show that template-synthesis can yield poly(3-methylthiophene) fibrils with conductivities as high as 6600 S $cm^{-1}$. This is the highest conductivity ever reported for a heterocyclic polymer.

## INTRODUCTION

The pores in nanoporous membranes can be used as templates for the synthesis of nanostructures (1-6). This approach has been used to produce nano cylinders (4,5), fibers (1,2), wires (6), and hollow tubules (3). We have coined the term "template synthesis" for this nanostructure fabrication process (3). We have recently shown that when the template method is used to synthesize nanoscopic conductive polymer fibrils, electronic conductivities along the axes of these fibrils can be dramatically higher than conductivities of bulk forms of the analogous polymers (1). Cahalane and Labes have observed a similar enhancement in conductivity for conductive polymer prepared via a derivative of the template method (7).

We are currently exploring the genesis of this enhanced electronic conductivity. We have discovered that there are both molecular and supermolecular differences between template-synthesized conductive polymers and conventional forms of these polymers. We will show in this and a succeeding paper (8) that these molecular and supermolecular differences are responsible for the enhanced electronic conductivities of the template-synthesized materials. This paper focuses on the supermolecular structures of template-synthesized polyheterocyclic fibrils and on the effects of supermolecular structure on conductivity in these fibrils.

The unique supermolecular feature of template-synthesized conductive polymer fibrils is preferential polymer chain

orientation (2). We have used a combination of polarized infrared absorption spectroscopy (2), DC and optical measurements of conductivity, and X-ray diffraction analyses to show that the polymer chains in narrow template-synthesized polyheterocyclic fibrils are preferentially oriented parallel to the axes of these fibrils. Because of this polymer chain alignment, these fibrils can be viewed as highly-ordered, self-assembling nanostructures. We have also found that through control of the synthetic conditions, template-synthesized poly(3-methylthiophene) fibrils with DC conductivities as high as 6600 S $cm^{-1}$ can be obtained. This is the highest conductivity ever reported for a heterocyclic polymer. These and related results are presented here.

## EXPERIMENTAL

Materials. Polypyrrole (PPY) and poly(3-methylthiophene) (PMT) were investigated in these studies. The starting materials, pyrrole and 3-methylthiophene (Aldrich, 99 %), were twice-distilled under nitrogen, immediately prior to use. Purified water, obtained by passing house distilled water through a Milli-Q (Millipore) water purification system, was used as the solvent for PPY synthesis. UV-grade acetonitrile (Burdick-Jackson) was used for the PMT syntheses. KBr was Aldrich IR grade. All other reagents were used as-received.

Nuclepore microporous polycarbonate filters (Nuclepore Corporation) were used as the template membranes (1,3,9). Nuclepore is available in a variety of pore diameters and densities. The specifications for the membranes used in these

studies are shown in Table I. The nominal values for the pore diameters and densities were supplied by the Nuclepore Corporation. The measured values were obtained from in house electron microscopic analyses of these membranes (9). Accurate values for pore diameter, pore density and membrane thickness are required to calculate fibril conductivity (1). We used our measured values (Table I) for these calculations. Nonporous polycarbonate sheet, identical to the sheet used to make Nuclepore membrane, was obtained from Mobay (Makrofol KG).

Polymer Syntheses. Two types of PMT and PPY were synthesized. The first was the fibrillar polymer which was synthesized using the Nuclepore membranes (Table I) as the template materials (1,3). The second was a "powderous" version of the polymer. The powderous versions were synthesized under identical conditions as the fibrillar materials but without the use of the template membrane. The powderous versions served as "controls" vs. which the properties of the fibrillar materials were evaluated. Electrochemically-synthesized film (10,11) was also used as a control material.

Fibril synthesis was accomplished using the apparatus shown in Figure 1 of reference (3). The Nuclepore membrane separated the monomer solution from a solution of a chemical oxidant, which served as the polymerization agent. For PPY, the monomer solution was 0.1 to 0.2 M aqueous pyrrole and the oxidant was 2 M aqueous $FeCl_3$. For PMT, the monomer solution was 0.4 to 0.6 M 3-methylthiophene and the oxidant was 2 to 3M $Fe(ClO_4)_3$ (solvent =

acetonitrile). All solutions were rigorously degassed with Ar. The $Fe^{3+}$ was added to the outer compartment (3) first. The monomer solution was added to the inner compartment (3) 10 to 20 sec. later. Polymerization was allowed to proceed for two hours. The membrane was then removed from the polymerization apparatus and rinsed with copious quantities of water or $CH_3CN$.

As indicated in our prior correspondences (1-3), template synthesis yields conductive polymer fibrils, which run through the pores in the Nuclepore membrane, and thin polymer films, which coat both faces of the membrane. The fibrils can be isolated by dissolution of the Nuclepore; however, the surface layers must be removed prior to dissolution. The surface layers were removed by polishing both faces of the membrane with 0.05 $\mu$m alumina powder. After polishing, the fibril/Nuclepore composite was ultrasonicated in water to the remove alumina powder. The Nuclepore was then dissolved by immersion in stirred $CH_2Cl_2$. The fibrils were collected by filtration (12) and rinsed with copious quantities of $CH_2Cl_2$, to remove traces of polycarbonate.

The powderous (control) versions of PPY and PMT were prepared by simply mixing the monomer solution with a solution of the polymerization agent. The polymer formed as a fine black precipitate; this precipitate was stirred in the mother liquor for ca. one hour and then collected by filtration. The polymer was then rinsed with copious quantities of either water or acetonitrile and dried in vacuo.

Transmission Electron Microscopy. Transmission electron

microscopic images were obtained by resuspending the isolated polypyrrole fibrils in $CH_2Cl_2$ and depositing a drop of the resulting suspension onto a porous carbon support (Electron Microscopy Center Texas A&M University). The suspension contained ca. 10 $\mu$g of polymer in 10 mL of $CH_2Cl_2$. Images were obtained using a Zeiss 10 transmission electron microscope at an accelerating voltage of 80 kV.

DC Conductivity. DC conductivity along the fibril axis was obtained by measuring the bulk resistance across the fibril/Nuclepore composite membrane (1,2). Resistances were measured using a two-point method based on the apparatus shown in Figure 1. Unless otherwise noted, the upper electrode was a 0.5 mm-dia. Pt wire sealed in glass. The lower electrode was a bed of 0.2 $\mu$m-diameter Ag particles (13). The ohm meter (Kiethley 190) was calibrated using high-precision resistors.

We initially completely removed the PPY or PMT surface layers prior to making resistance measurements on the fibril/Nuclepore composites. However, after removal of the surface layers, it proved impossible to obtain reproducible resistance data for the composite membrane. Excellent reproducibility was obtained when the surface layers were left intact. Clearly, the surface layers function as strongly adherent electrical contacts to the fibrils and thus minimize contact resistance problems.

While leaving the surface layers intact minimized contact resistance, it is in principle possible that the measured

composite membrane resistance is a convolution of the resistances of the fibrils (wanted) and the resistances of these surface layers (unwanted). To circumvent this problem we adopted the following compromise protocol: Rather than completely removing the surface layers, these layers were thinned by polishing with a laboratory tissue (14). Electron microscopic analyses showed that after this (less abrasive) polish, the surface layers were less than 200 nm thick (15). Appendix A shows that these ultrathin surface layers do not contribute to the membrane resistance.

A pressure of ca. $2x10^3$ psi was applied between the upper and lower electrodes during the resistance measurements. This pressure was arrived at via a study of the effect of applied pressure on the measured resistance of the fibril/Nuclepore composite. An IR pellet press was used to control the applied pressure. The measured resistance initially decreased with pressure but then leveled at pressures above ca. $1x10^3$ psi (15). The higher resistance, at lower pressures, undoubtedly reflects a contribution from contact resistance.

At pressures above ca. $1x10^3$ contact resistance is negligibly small. Figure 2a proves this point; this figure shows a plot of measured resistance for a stack of fibril/Nuclepore composite membranes vs. the number of membranes in the stack. This plot is linear and has an intercept of zero. If contact resistance were significant, a positive intercept would have been obtained. Defining the electrode area presents another potential

source of error (see Appendix A). We assume that the relevant area is just the area of the upper, Pt wire, electrode. If this is true, then a plot of measured resistance vs. the inverse of the electrode area should be linear, with zero intercept. Figure 2b shows that this is indeed the case.

Typical raw resistance data for several fibril/Nuclepore composites are shown in Table II. The conductivity along a single fibril can be calculated from these data (see Appendix B), provided the number and diameter of fibrils in the membrane are known (Table I). As a further test of the validity of our two-point method, we obtained analogous resistance data after chemically "undoping" the conductive polymer fibrils (Table II). Undoping was accomplished by exposing the membranes to 2 M NaOH (PPY) (16) or 0.2 M $NaBH_4$ (in $CH_3CN$,PMT) (17). Because the undoped fibril is an electronic insulator (16,17), the resistance of the composite membranes should increase dramatically. Table II shows that this is, indeed, the case.

Four-point measurements of electronic conductivity are preferable to two-point measurements. However, it is impossible to obtain four-point measurements on our nanoscopic fibrils. Contact resistance is the most significant problem in a two-point measurement; we have show that contact resistance is negligible (Figure 2a). There are other potential problems. For example, we assume that all of the pores are filled with contiguous conductive polymer fibrils; electron microscopic evidence suggests that this is, indeed, the case. However, if it were not

the case, the real fibril conductivities would be higher than the conductivities report here. The same can be said if contact resistance were a problem or if the surface layers contribute to the membrane resistance (Appendix A). Hence, the DC conductivities reported here should be viewed as minimum values. Finally, it is important to point out that optical measurements of electronic conductivity (see below) corroborate the DC conductivities obtained from our two-point measurements.

Conductivities of the powderous polyheterocyclic samples were obtained by pressing the powders into pellets; a pressure of $2x10^6$ PSI was used. A standard four-point method was used to obtain the conductivities of the pressed pellets (18). Conductivities for electrochemically-synthesized films were taken from the literature (11,12). The conductivities reported in these papers (11,12) are the highest conductivities reported for electrochemiclly-synthesized PPY and PMT.

Optical Conductivity. As discussed by Chien, the infrared absorption spectrum for an electronically conductive polymer can be used to calculate an optical conductivity ($\sigma_{opt}$) for the polymer (19). Such calculations make use of the Drude approximation (20). A discussion of the assumptions involved in the Drude model can be found in (19-21). The Drude model has been used to calculate $\sigma_{opt}$ values for a variety of conductive polymers (22-24). The limitations in the applicability of this model to conductive polymers have been discussed (22-24).

According to the Drude model, $\sigma_{opt}$ is related to the

absorption coefficient ($\alpha$) via (19)

$$\sigma_{opt} = (\alpha^2 c^2)/8\pi\omega \quad (1)$$

where c is the speed of light and $\omega$ is the frequency of light employed. The absorption coefficient can be obtained from the experimental absorbance (A) via

$$A = \alpha b \quad (2)$$

where b is the film thickness.

Optical conductivities were obtained for 600 nm and 30 nm-diameter PPY fibrils and for powderous PPY. Samples were prepared by mixing measured quantities of the isolated fibrils (or powderous polymer) with measured quantities of KBr and pressing pellets; pellets were pressed at $2x10^6$ psi. Infrared absorption data were obtained on these samples using a Mattson Galaxy 4021 FTIR. A pellet which was devoid of polymer served as the reference.

The relevant thickness (Equation 2) for these composite (polymer plus KBr) samples is not the thickness of the pellet but rather the effective thickness of the polymer dispersed within the pellet. This effective thickness was calculated from the known weight of polymer in the pellet, the area of the pellet, and the density of PPY. Densities were obtained by pressing pellets of weighed quantities of the polymer and then measuring the volume of the resulting pellets. (KBr was not added to these pellets.) A density for both fibrillar and powderous PPY of $1.44\pm0.05$ g $cm^{-3}$ was obtained. This agrees well with a density of 1.48 g $cm^{-3}$ reported by Hasegawa et al. (23).

X-Ray Diffraction. Diffraction data were obtained for both powderous and fibrillar PPY samples. The fibrillar samples were obtained by dissolving the template membrane and collecting the fibrils by filtration. PPY fibrils with diameters of 30 and 400 nm investigated. Diffraction data were obtained with a Seifert-Scintag Pad diffractometer using $CuK_\alpha$ radiation ($\lambda$ = 0.15418 nm).

Polarized Infrared Absorption Spectroscopy (PIRAS). PIRAS is a classical technique for investigating chain orientation in polymers (25,26). We have recently used PIRAS to prove that the polyacetylene chains in template-synthesized polyacetylene fibrils are oriented parallel to the axes of these fibrils (2). PIRAS data for the PPY fibrils were obtained as follows:

Prior to template synthesis, the Nuclepore membrane was placed in the FTIR sample holder and background absorbance spectra, for both polarizations employed (see below), were obtained. A typical background spectrum is shown in Figure 3 (lower curve). Template synthesis of PPY was then conducted without removing the membrane from the sample holder. (This wa done so that absorbance data for the fibril/Nuclepore composite could be obtained from the same spot on the membrane used for the background spectrum.) After template-synthesis, the surface PPY layers were removed by polishing with alumina powder.

The fibril/Nuclepore composite was then placed back in the spectrometer and spectra were, again, obtained for each polarization. A typical composite membrane spectrum is shown in Figure 3 (upper curve). A comparison of the spectra in Figure 3

shows that the virgin Nuclepore membrane has essentially no absorbance at 1550 $cm^{-1}$ whereas the composite shows a clearly discernable peak at this energy. This peak is due to the antisymmetric ring stretching mode of the monomer units within the PPY chain (27). While this peak appears weak (relative to the Nuclepore peaks), subtraction of the background spectrum yielded PPY spectra which were essentially identical to spectra obtained from the isolated fibrils (Figure 4 (28)). Spectra like that shown in Figure 4 were obtained (for both of the polarizations used, see below) for PPY fibrils with diameters of 600, 400, 50, and 30 nm.

The polarizations used for the PIRAS analysis are shown in Figure 5. An Au wire grid polarizer was used to control polarization. The polarization labeled $I_{\perp}$ is orthogonal to the axes of the PPY fibrils. The integrated absorbance by the PPY fibrils of this polarization is labeled $A_{\perp}$. The polarization vector for the beam labeled $I_{30}$ makes an angle of 30° with respect to the fibril axes. The integrated absorbance by the fibrils of this polarization is labeled $A_{30}$. In general, if $A_{\perp} = A_{30}$, the PPY chains are randomly oriented within the fibrils; nonequal integrated absorbencies indicates that the polymer chains show some preferred spatial orientation (25,26).

The integrated absorbencies can be used to obtain a parameter called the dichroic ratio, $R = A_{\parallel}/A_{\perp}$, where $A_{\parallel}$ is the integrated absorbance intensity for a beam polarized parallel to the fibril axis (29). The dichroic ratio quantitatively

describes the extent of polymer chain orientation within a sample (26,27). $A_{30}$ is related to $A_{||}$ and $A_{\perp}$ via (26)

$$A_{30} = A_{||} \cos^2(30°) + A_{\perp} \sin^2(30°) \quad (3)$$

Dividing both sides of Equation 3 by $A_{\perp}$ and rearranging yields

$$R = A_{||}/A_{\perp} = 1/3(4A_{30}/A_{\perp} - 1) \quad (4)$$

## RESULTS AND DISCUSSION

Electron Microscopy. A transmission electron micrograph of isolated 30 nm-diameter polypyrrole (PPY) fibrils is shown in Figure 6. These fibrils show good monodispersity in both length and diameter. The length is determined by the thickness of the host membrane, in this case 10 $\mu$m; the width is determined by the diameter of the pores in the host membrane. The aspect ratio for these fibrils is ca. 333. The fibrils have good mechanical strength as evidenced by the fact that they withstand ultrasonification. Finally, note that a number of the fibrils in Figure 6 appear to rather strongly bent; this also suggests that these fibrils are strong and flexible.

DC Conductivity ($\sigma_{DC}$). Plots of $\sigma_{DC}$ vs. fibril diameter, for fibrils synthesized at two different temperatures, are shown in Figure 7. In agreement with our previous study (1), $\sigma_{DC}$ values for the smallest fibrils increase as the fibril diameter decreases. The data in the lower curve were obtained from fibrils synthesized at 23° C. The highest $\sigma_{DC}$ achieved at this temperature was 1050 S $cm^{-1}$ (30 nm-diameter fibrils). The upper curve in Figure 7 was obtained for fibrils synthesized at 0° C. These fibrils show dramatically higher conductivities than the

fibrils synthesized at 23° C. An analogous effect of synthesis temperature was observed for PMT (Table III).

Table III presents the highest conductivities obtained, to date, for 30 nm-diameter PPY and PMT fibrils. (We have not yet investigated smaller fibrils.) These data clearly illustrate the effect of synthesis temperature on $\sigma_{DC}$ (30). (The PIRAS data discussed below provide an explanation for this observation.) The conductivity of 6,600 S $cm^{-1}$ for the PMT fibrils synthesized at -26° C, is the highest conductivity ever reported for a polyheterocyclic. These 30 nm-diameter PMT fibrils are over an order of magnitude more conductive than the best electrochemically-synthesized films (11). The 30 nm-diameter PPY fibrils synthesized at 0° C are ca. one order of magnitude more conductive than the best electrochemically-synthesized film (10). Our chemically-synthesized powders showed conductivities from 10 to 50 S $cm^{-1}$, which is typical for PMT and PPY (31,32).

Optical Conductivity ($\sigma_{opt}$). The intent of these studies was to obtain independent verification of the enhanced DC conductivities of the fibrillar polymers. IR spectra for fibrillar and powderous PPY are shown in Figure 8. These spectra show the featureless rise in absorbance with energy which is characteristic of PPY in this energy region (22). All of the samples contained identical quantities of PPY; however, the absorbance for the 30 nm-diameter fibrils is significantly higher than absorbencies for the powderous material or the 600 nm-diameter fibrils. This suggests that the 30 nm-diameter fibrils

are more conductive (Equation 1).

Optical conductivities calculated from the IR data are shown in Table IV. In agreement with previous analyses of this type (22), $\sigma_{opt}$ increases with energy over this region (vide infra). Most importantly, note that at any frequency, $\sigma_{opt}$ for the 30 nm-diameter fibrils are over an order of magnitude higher than the corresponding $\sigma_{opt}$'s for either the 600 nm-diameter fibrils or the PPY powder. These data corroborate the DC conductivity measurements (Figure 7, Table III).

As indicated above, the objective of these experiments was to obtain corroborating evidence for the increased DC conductivities of our nanoscopic polyheterocyclic fibrils. This was accomplished by comparing optical conductivities for 30 nm fibrils with analogous $\sigma_{opt}$'s for powders and larger fibrils. Other workers have, however, attempted to make absolute comparisons between the optical and DC conductivities (23,24). Such comparisons are, in principle, possible because the Drude model predicts that $\sigma_{opt}$ is inversely proportional to frequency, and approaches $\sigma_{DC}$ at zero frequency (21,24). Thus, optical and DC conductivities can, in principle, be compared by comparing $\lim_{w \to o}(\sigma_{opt})$ with $\sigma_{DC}$.

We (Table IV) and others (21,22) have found, however, that PPY does not adhere to this simple Drude-model prediction. (Note that $\sigma_{opt}$ is proportional, rather than inversely proportional, to frequency (Table IV).) Polyacetylene shows analogous "anti-Drude" optical conductivity data (24). This anti-Drude behavior

is probably caused by defects in the polymer chains (24). Because of this anti-Drude behavior $\lim_{w \to o}(\sigma_{opt})$ is less than $\sigma_{DC}$ (24), making comparisons between $\sigma_{opt}$ and $\sigma_{DC}$ problematic. Finally, it is worth noting that the maximum absorbance for PPY is in the near IR (22), an energy region not accessed by this study. Evidence for this (missing) maximum can be seen in the data in Table IV. Thus, our PPY samples could show higher optical conductivities than the values presented in Table IV.

Investigations of the Supermolecular Structure. The remainder of this paper will be devoted to understanding why the nanoscopic conductive polymer fibrils show higher conductivities than electrochemically-synthesized films or chemically-synthesized powders. We will show, below, that part of this enhanced conductivity is a supermolecular effect. We will show in Part II of this series that molecular effects are also contribute to these enhanced conductivities (8).

1. X-Ray Diffraction. PPY shows a broad and weak X-ray reflection corresponding to a Bragg spacing of 0.34 nm (30); this is usually the only feature in the diffractogram, indicating that PPY is completely amorphous. Diffractograms for our powderous PPY show only this high-angle reflection (Figure 9a); diffractograms for 400 nm PPY fibrils are identical, indicating that these large fibrils are also completely amorphous. In contrast, diffractograms for our 30 nm-diameter PPY fibrils show a second, and more intense, reflection corresponding to a Bragg spacing of 1.47 nm (Figure 9b; note that the x-axis scale is

different than 9a). This new reflection indicates that the polymer chains in these nanoscopic PPY fibrils show supermolecular order not present in conventional PPY (30).

What is the nature of this enhanced order? Yamaura et al. have recently conducted X-ray diffraction analyses on stretched PPY films (30). This stretched material also showed a low angle reflection corresponding to a Bragg spacing of ca. 1.5 nm. They suggest that stretching causes the PPY chains to align and that this alignment accounts for the new X-ray reflection (30); this is a common observation for stretch-oriented polymers (33). The similarity between the diffraction data for stretched and template-synthesized PPY suggests that template-synthesis in nanoscopic pores also causes the polymer chains to align.

This conclusion is in perfect accord with the DC conductivity data. It is well known that aligning conductive polymer chains (typically by stretching) enhances conductivity along the alignment axis (34). Hence, the X-ray diffraction and conductivity data suggest that the polymer chains in our narrowest fibrils are aligned parallel to the fibril axes. The PIRAS data strongly support this conclusion.

2. Polarized Infrared Absorption Spectroscopy (PIRAS). PIRAS is the ideal technique for investigating chain orientation in polymers. Typical PIRAS spectra, in the region of the PPY antisymmetric ring stretching mode, are shown in Figure 10. Note first that the large PPY fibrils (600 and 400 nm) absorb both the perpendicular and 30°-polarizations to the same extent.

Consequently, the dichroic ratios for these large fibrils are unity, Table V. This indicates that the polymer chains in these large fibrils show no preferred spatial orientation. This is in perfect accord with the X-ray diffraction and conductivity data for such large fibrils.

In contrast, the narrow (30 and 50 nm) PPY fibrils preferentially absorb the perpendicular polarization (Figure 10). The dichroic ratios obtained from these spectra are shown in Table V; these nonunity dichroic ratios indicate that the polymer chains in these extremely narrow fibrils show a preferred spatial orientation. Furthermore, the extent of dichroism is higher in the 30 nm fibrils than in the 50 nm fibrils (Table V). This suggests that the polymer chains in the 30 nm fibrils are more strongly oriented than in the 50 nm fibrils. This is in perfect accord with the conductivity data (Figure 7, note that the 30 nm fibrils are more conductive) and the X-ray diffraction data.

As indicated in Figure 7 and Table III, PPY fibrils synthesized at 0° are more conductive than PPY fibrils synthesized at room temperature. PIRAS provides a partial (30) explanation for this observation. As shown in Table V, the nanoscopic fibrils synthesized at the lower temperature show greater dichroism than analogous fibrils synthesized at room temperature. These data suggest that the fibrils synthesized at the low temperature are more strongly oriented; this enhanced orientation makes these low-temperature fibrils more conductive.

The conductivity, X-ray diffraction, and PIRAS data all tell

a coherent story about our template-synthesized polyheterocyclic fibrils - These various data suggest that the polymer chains in the narrowest fibrils are preferentially oriented parallel to the fibril axis and that the extent of orientation increases as the diameter of the fibril and the synthesis temperature decrease.

## CONCLUSIONS

Template-synthesized conductive polymer fibrils (1) and tubules (3) can be viewed as highly-ordered self-assembling nanostructures. Understanding the mechanism by which supermolecular order is self-assembled into these structures may have important implications for other highly-ordered self-assembling systems (e.g. biological systems). We have formulated a simple (preliminary) model for the genesis of enhanced supermolecular order in the template-synthesized polymeric nanostructures. We conclude this paper with this model.

It is well known that nascent, chemically-synthesized, PPY chains adsorb to various polymeric surfaces (35). For example, Kuhn et al. have shown that PPY-coated fabrics (e.g. polyester, cotton, polypropylene) can be obtained by immersing the fabric into a solution containing pyrrole and $Fe^{3+}$ (35). Their data suggest that the adsorbing species is an oligomeric PPY chain and not the monomer or the oxidant (35). An analogous adsorption phenomenon occurs during template synthesis. Indeed, we have recently shown that, because of the preferential adsorption of the nascent PPY chains to the pore walls in Nuclepore, template synthesis can yield organic microtubules (3).

We believe that this adsorption process is the key to understanding the genesis of polymer chain orientation in the template-synthesized polyheterocyclic fibrils. We first postulate that strong (i.e. irreversible) adsorption between the nascent polyheterocyclic chain and a surface can only occur if the chain (or a segment thereof) can adsorb to the surface along the entire chain (or segment) length; i.e. we assume that the total adsorption energy is some function of the sum of the adsorption energies of the individual monomer units that make up the chain, and that a number of consecutive monomer units must adsorb for irreversible adsorption to occur.

The ability of the polyheterocyclic chain to adsorb along the entire chain (or segment) length is potentially hindered by the fact that these chains are very stiff (36). To understand why stiffness is a potential problem, imagine a pencil in a large drain pipe (diameter of pipe > length of pencil). The only way the entire length of the (stiff) pencil can come into contact with the curved inner surface of the pipe is if the pencil is aligned parallel to the axis of the pipe. At all other orientations, the pencil contacts the wall of the pipe in only two places - the beginning and end of the pencil.

According to the above analogy, if the persistence length of a polyheterocyclic chain is large relative to the radius of curvature of the pore wall, the chain will be forced to adsorb parallel to the pore axis, because this is the only configuration which will allow all of the monomer units in the chain (or chain

segment) to interact with the pore wall. This will be the case for very small-diameter pores. In contrast, if the pore diameter is very large, the radius of curvature is small, and the wall will look flat to the adsorbing chain. In this case, the chain can adsorb in any orientation and still achieve total contact with the pore wall. According to this simple model, polyheterocyclic chains will be forced to adsorb parallel to the axis of the pore in small pores but can adsorb at any orientation in large pores. This conclusion is in complete accord with our experimental data.

We are currently attempting to verify this simple model. We are also attempting to synthesize even more highly-conductive fibrils. What is the ultimate conductivity achievable in a simple heterocyclic polymer? We would like to be able to answer this question.

Acknowledgements. This work was supported by the Office of Naval Research.

## REFERENCES AND NOTES


1. Cai, Z.; Martin, C.R. J. Am. Chem. Soc. 1989, 111, 4138.
2. Liang, W.; Martin, C.R. J. Am. Chem. Soc. In press.
3. Martin, C.R.; Van Dyke, L.S.; Cai, Z.; Liang, W. J. Am. Chem. Soc. 1990, 112, 8976.
4. Tierney, M.J.; Martin, C.R. J. Phys. Chem. 1989, 93, 2878.
5. Penner, R.M.; Martin, C.R. J. Electrochem. Soc. 1986, 133, 2206.
6. Williams, W.D.; Giordano, N. Rev. Sci. Instru. 1984, 55(3), 410.
7. Cahalane, W.; Labes, M.M. Chem. Materials, 1989, 1, 519.
8. Cai, Z.; Liang, W.B.; Martin, C.R. In prep.
9. Cheng, I.F.; Whiteley, L.D.; Martin, C.R. Anal. Chem. 1989, 61, 762.
10. Yamaura, M.; Hagiwara, T.; Iwata, K. Synth. Met. 1988, 26, 209.
11. Sato, M.; Tanaka, S.; Kaeriyama, K. Synth. Met. 1986, 14, 279.
12. Van Dyke, L.S.; Martin, C.R. Langmuir, 1990, 6, 1118.
13. We initially used two Pt wires as the electrodes; however, unless the surfaces of these two solid electrodes were perfectly parallel, good contact with both faces of the membrane could not be achieved. The particle bed electrode obviates this problem because it is like a fluid and thus can conform to the lower membrane surface, regardless of angle.

14. A Kim-Wipe was wetted with water and each surface of the membrane was hand polished for several minutes. The surface of the Kim-Wipe darkened during polishing, indicating that polymer had been removed from the membrane. The membrane was then rinsed with copious qunatities of water.
15. These data are available upon request.
16. Inganas, O.; Erlandsson, R.; Nylander, C.; Lundstrom, I. J. Phys. Chem. Solids, 1984, 45, 427.
17. When PMT is treated in this way it losses the dark coloration characteristic of the doped polymer and, as indicated in Table II, the resistance increases dramatically.
18. Penner, R.M.; Martin, C.R. J. Electrochem. Soc. 1986, 133, 310.
19. Chien, J.C.W. Polyacetylene, Academic Press, NY, 1984, pp. 551-552.
20. Simon, J.; Andre, J.J. Molecular Semiconductors, Springer-Verlag, NY, 1985, pp. 8-17.
21. Abeles, F. Optical Properties of Solids, North-Holland, Amsterdam, 1972, pp. 143-145.
22. Yakushi, K.; Lauchlan, L.J.; Clarke, T.C.; Street, G.B. J. Chem. Phys. 1983, 79, 4774.
23. Hasegawa, S.; Kamiya, K.; Tanaka, J.; Tanaka, M. Synth. Met. 1986, 14, 97.
24. Fincher, C.R., Jr.; Ozaki, M.; Tanaka, M.; Peebles, D.; Lauchlan, L.; Heeger, A.J.; MacDiarmid, A.G. Phys. Rev. B, 1979, 20, 1589.

25. Monnerie, L. in Ward, I.M., Ed. Developments in Oriented Polymers, Elsevier, London, Vol. 2, 1987.

26. Zbinden, R. Infrared Spectroscopy of High Polymers, Academic Press, NY, 1964, p. 186.

27. Lord, R.C.; Miller, F.A. J. Chem. Phys. 1942, 10, 328.

28. As can be seen in Figure 4, the Nuclepore membrane shows an extremely intense series of bands at ca. 1200 $cm^{-1}$. A vestige of this band can be seen in the background-corrected spectrum (upper curve in Figure 5) at ca. 1250 $cm^{-1}$. This uncorrected background peak is, however, so far removed from the 1550 $cm^{-1}$ band used in the PIRAS analysis that its presence is not a problem.

29. The ideal geometry for this analysis would be to impinge the IR radiation on the edge of the membrane so that a truly parallel polarization vector could be achieved. Because the membranes are so thin (Table I), this configuration is impractical.

30. Yamaura, M.; Hagiwara, T,; Hirasaka, M.; Demura, T.; Iwata, K. Synth. Met. 1989, 28, 157.

31. Street, G.B.; in Handbook of Conducting Polymers, Skotheim, T.A. Ed., Marcel Dekker, NY, Vol. 1, p.282.

32. Tourillon, G.; Ibid, p. 325.

33. Shastri, R.; Roehrs, H.C.; Brown, C.N.; Dollinger, S.E. in Barrier Polymers and Structures, Koros, W.J., Ed., ACS Sym. Ser. 423, ACS, Washington, DC, 1990, p. 240.

34. Kirppka, M.; Doi, T. Synth. Met. 1987, 17, 209.

35. Gregory, R.V.; Kimbrel, W.C.; Kuhn, H.H. Synth. Met. 1989, 28, C823.

36. Polyheterocyclic chains are stiff because they are composed of five-membered rings with double bonds between the rings.

Table I. Characteristics of the Nuclepore membranes used in these studies

| Pore diameter (nm) | | Porosity[a] | | Thickness (μm)[b] |
|---|---|---|---|---|
| Nominal[c] | Measured[d] | Nominal[c] | Measured[d] | |
| 30 | 30 ± 4 | 0.0021 | 0.0018 | 10.0±1 |
| 50 | 50 ± 4 | 0.0059 | 0.0067 | 10.5 |
| 100 | 100 ± 10 | 0.0233 | 0.0250 | 11.0 |
| 200 | 200 ± 20 | 0.090 | 0.084 | 14.5 |
| 600 | ---- | 0.081 | ---- | 15.0 |
| 800 | 800 ± 70 | 0.140 | 0.14 | 15.5 |
| 1000 | ---- | 0.145 | ---- | 15.0 |

[a] Fractional pore area.
[b] Measured using a digital micrometer.
[c] From Nuclepore Corp. product literature.
[d] Measured from electron micrographs of the surfaces of the membranes.

**Table II.** Typical raw resistance data for several fibril/Nuclepore composite membranes.

| Polymer[a] | Fibril diameter (nm) | Resistance (Ω)[b] Doped | Undoped |
|---|---|---|---|
| PPY | 30 | 0.25 | 1400 |
| '' | 200 | 0.14 | 2700 |
| '' | 800 | 0.09 | --- |
| PMT | 30 | 0.17 | $1x10^6$ |
| '' | 200 | 0.24 | --- |
| '' | 600 | 0.39 | $5x10^6$ |

[a] Polymers were synthesized at 25°C.
[b] Background resistance noise was ±0.005 Ω.

Table III. Highest DC conductivities obtained to date for 30 nm-diameter polyheterocyclic fibrils.

| Polymer | Synthesis temperature (°C) | Conductivity ($\Omega^{-1}cm^{-1}$) |
|---|---|---|
| PPy[a] | 23 | 1050 |
| '' | 0 | 4100 |
| PMT[b] | 23 | 1505 |
| '' | 0 | 2731 |
| '' | -26 | 6597 |

[a] Pyrrole concentration = 0.2 M; $FeCl_3$ concentration = 2 M.
[b] 3-methylthiophene concentration = 0.6 M; $Fe(ClC_4)_3$ concentration = 3 M.

**Table IV.** Absorption coefficient ($\alpha$) and optical conductivity ($\sigma_{opt}$) for PPY fibrils and powder[a].

| Energy ($cm^{-1}$) | Powder | | 600 nm fibril | | 30 nm fibril | |
|---|---|---|---|---|---|---|
| | $\alpha$ ($cm^{-1}$) | $\sigma_{opt}$ ($Scm^{-1}$) | $\alpha$ ($cm^{-1}$) | $\sigma_{opt}$ ($Scm^{-1}$) | $\alpha$ ($cm^{-1}$) | $\sigma_{opt}$ ($Scm^{-1}$) |
| 2000 | $6.1x10^3$ | 4.0 | $4.6x10^3$ | 2.2 | $3.2x10^4$ | 108 |
| 2500 | $8.7x10^3$ | 6.4 | $7.7x10^3$ | 5.1 | $4.3x10^4$ | 157 |
| 3333 | $1.2x10^4$ | 9.1 | $1.1x10^4$ | 7.9 | $5.6x10^4$ | 199 |
| 3535 | $1.4x10^4$ | 12.5 | $1.3x10^4$ | 9.4 | $6.7x10^4$ | 271 |
| 4000 | $1.7x10^4$ | 14.3 | $1.5x10^4$ | 12.4 | $7.7x10^4$ | 314 |
| 11000 | $2.7x10^4$ | 14.9 | $1.9x10^4$ | 7.0 | $1.8x10^5$ | 640 |
| 12500 | $2.2x10^7$ | 10.0 | $1.7x10^4$ | 5.6 | $1.5x10^5$ | 427 |

[a] All samples were synthesized at 23°C.

**Table V.** Dichroic ratios ($R = A_{||}/A_{|}$) for polypyrrole fibrils synthesized at different temperatures.

| Fibril Diameter (nm) | Synthesis Temperature 0 °C | 23 °C |
|---|---|---|
| 0.6 μm fibril | --- | 1.01±0.04 |
| 0.4 μm fibril | 0.95±0.04 | 0.97 |
| 0.05 μm fibril | 0.40 | 0.61 |
| 0.03 μm fibril | 0.11 | 0.17 |

FIGURE CAPTIONS

Figure 1. Schematic of apparatus used to conduct two-point conductivity measurements on the fibril/Nuclepore composite membranes.

Figure 2. A. Plot of resistance for a stack of fibril/Nuclepore composite membranes vs. total thickness of the stack. B. Plot of resistance of a fibril/Nuclepore composite membrane vs. inverse of area of (upper) Pt disk electrode (see Figure 1).

Figure 3. PIRAS data for - Upper, virgin Nuclepore membrane (50 nm pore diameter). Lower, the same membrane after template-synthesis of PPY fibrils and removal of the surface layers.

Figure 4. Upper, PPY IR spectrum obtained after subtraction of background Nuclepore spectrum from composite membrane spectrum (see Figure 3). Lower, (shown for comparison) analogous spectrum of isolated PPY fibrils in KBr pellet.

Figure 5. Configuration and polarizations used for PIRAS studies.

Figure 6. Transmission electron micrograph of 30 nm-diameter template-synthesized PPY fibrils.

Figure 7. Plot of fibril conductivity vs. fibril diameter for PPY fibrils synthesized at two different temperatures.

Figure 8. FTIR spectra of isolated PPY fibrils and PPY powder in KBr pellets.

Figure 9. X-ray diffractograms for A. 30 nm-diameter template-synthesized PPY fibrils. B. PPY powder.

Figure 10. PIRAS spectra for PPY fibrils of various diameters.

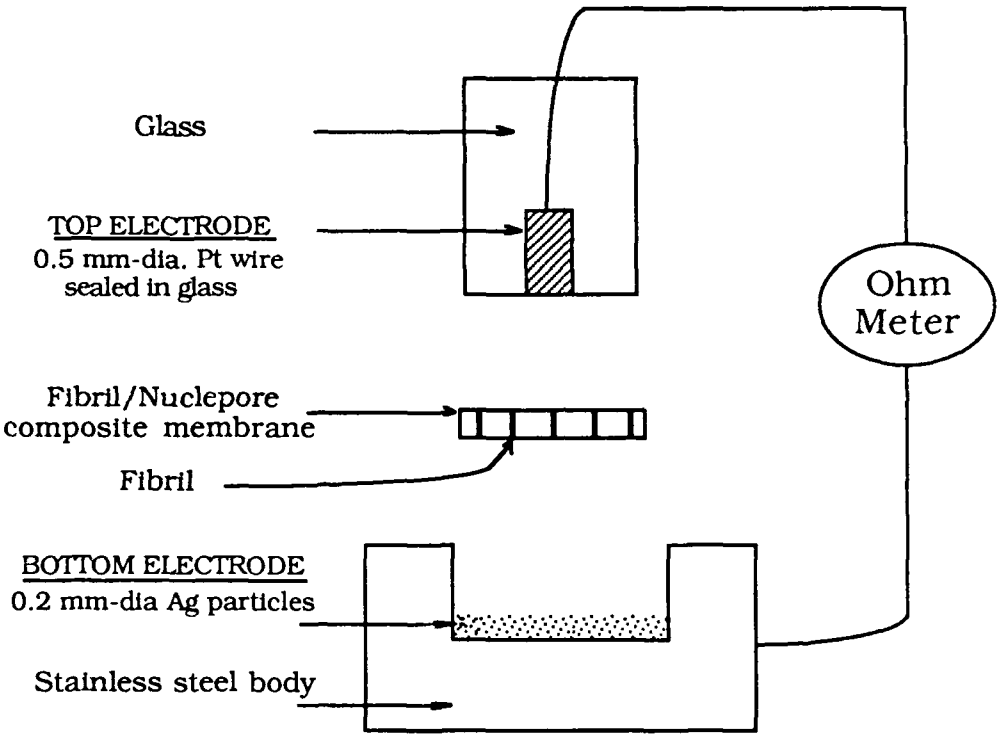
Glass
TOP ELECTRODE
0.5 mm-dia. Pt wire
sealed in glass
Ohm
Meter
Fibril/Nuclepore
composite membrane
Fibril
BOTTOM ELECTRODE
0.2 mm-dia Ag particles
Stainless steel body

Fig. 1

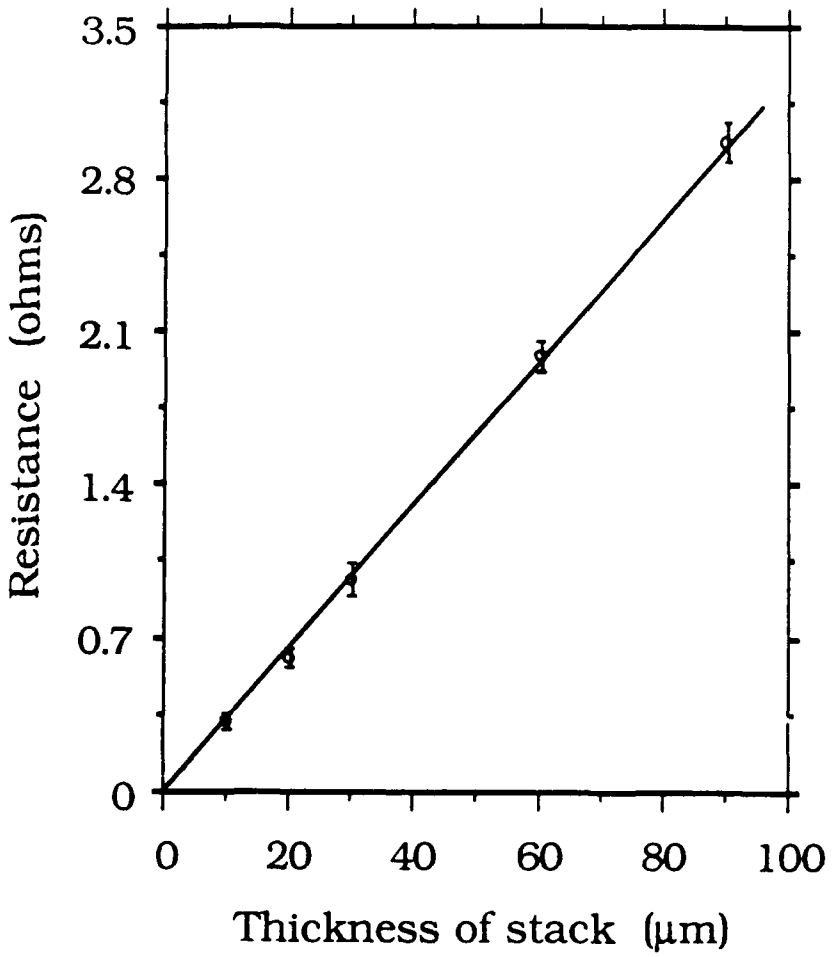
3.5
2.8
2.1
1.4
0.7
0
Resistance (ohms)
0
20
40
60
80
100
Thickness of stack (μm)

Fig. 2a

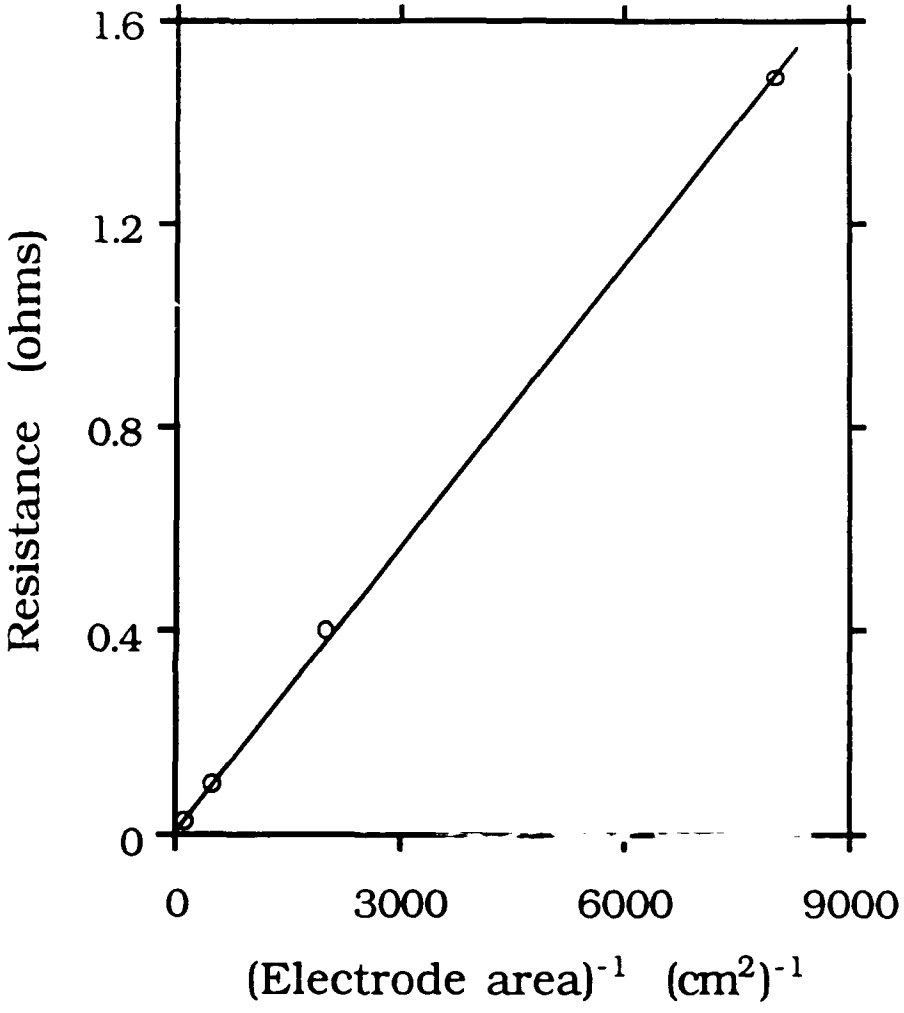
1.6
1.2
0.8
0.4
0
Resistance (ohms)
0
3000
6000
9000
(Electrode area)$^{-1}$ (cm$^2$)$^{-1}$

Fig. 26

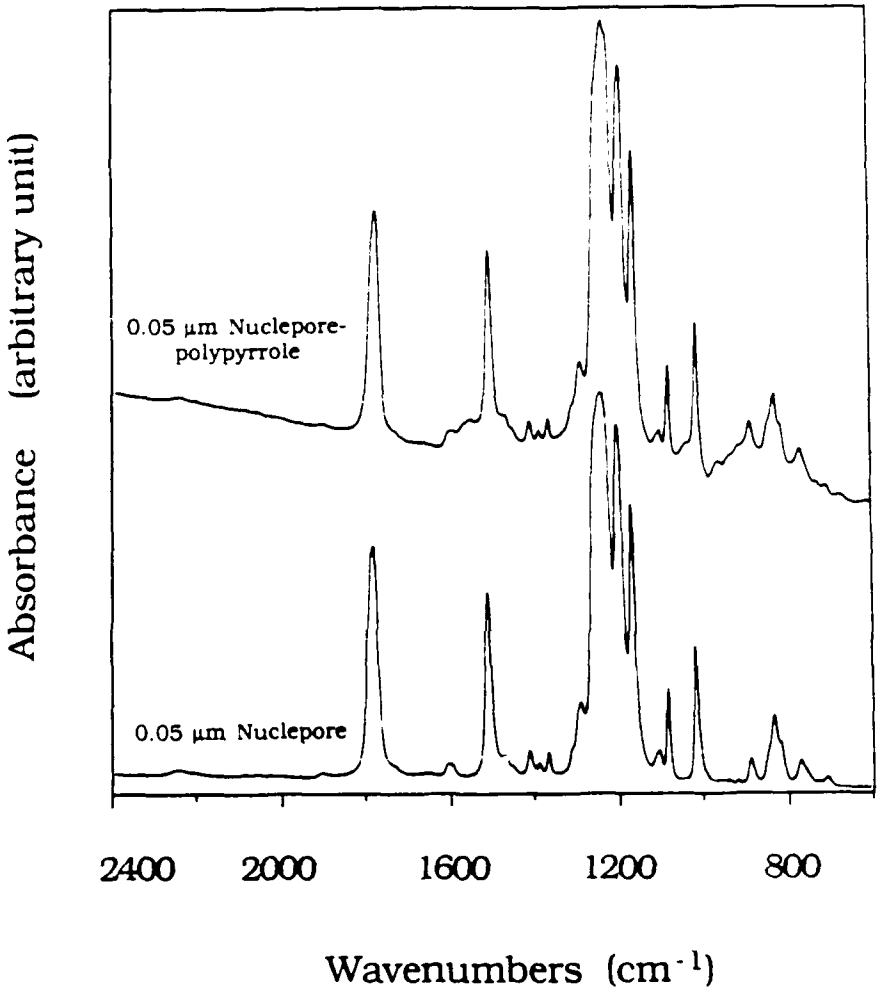
Absorbance (arbitrary unit)
0.05 µm Nuclepore-polypyrrole
0.05 µm Nuclepore
2400
2000
1600
1200
800
Wavenumbers (cm-1)

Fig. 3

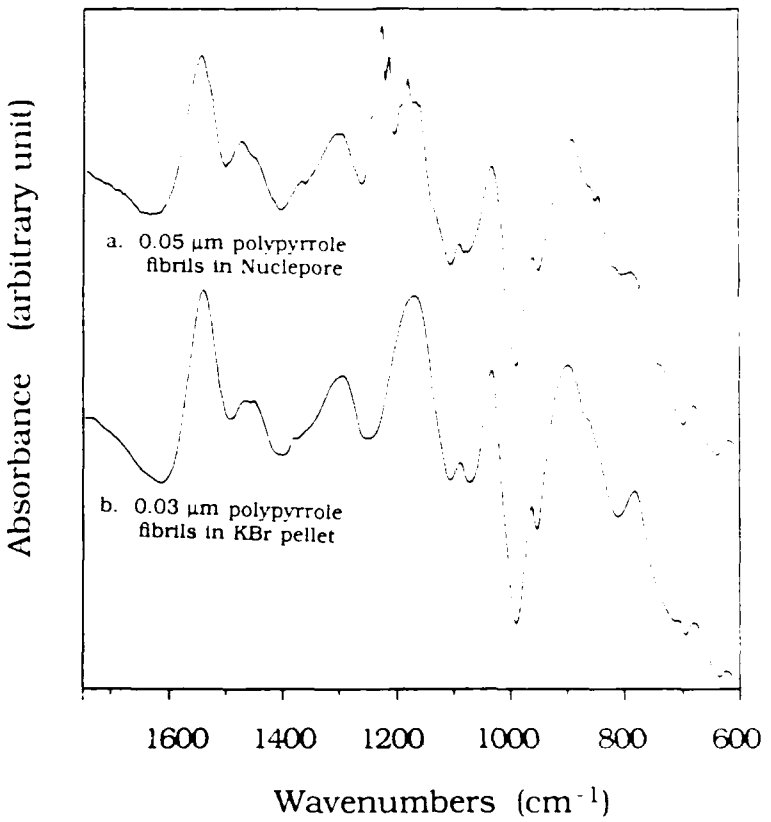
Absorbance (arbitrary unit)
a. 0.05 µm polypyrrole fibrils in Nuclepore
b. 0.03 µm polypyrrole fibrils in KBr pellet
1600
1400
1200
1000
800
600
Wavenumbers (cm⁻¹)

Fig. 4

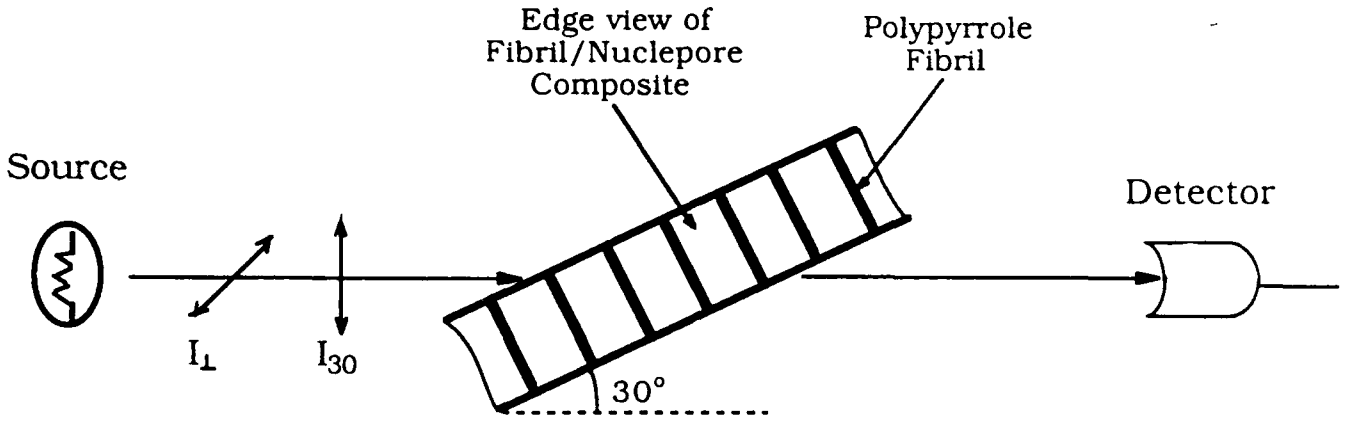
Edge view of
Fibril/Nuclepore
Composite
Polypyrrole
Fibril
Source
Detector
$I_\perp$
$I_{30}$
30°

Fig. 5

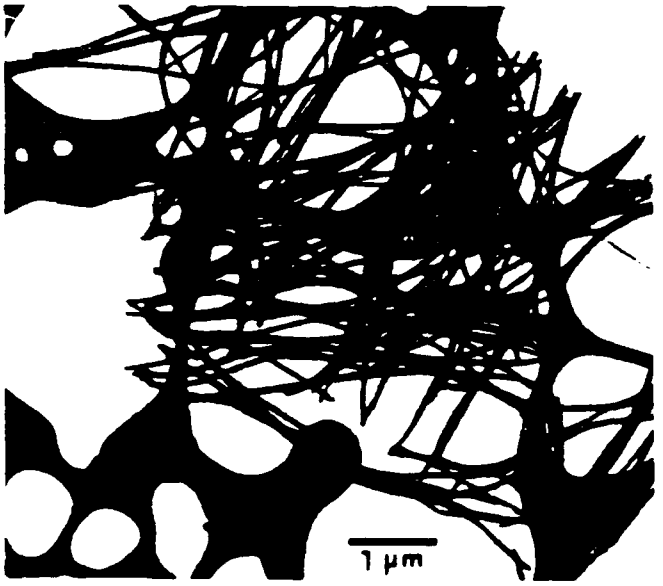


Fig. 6

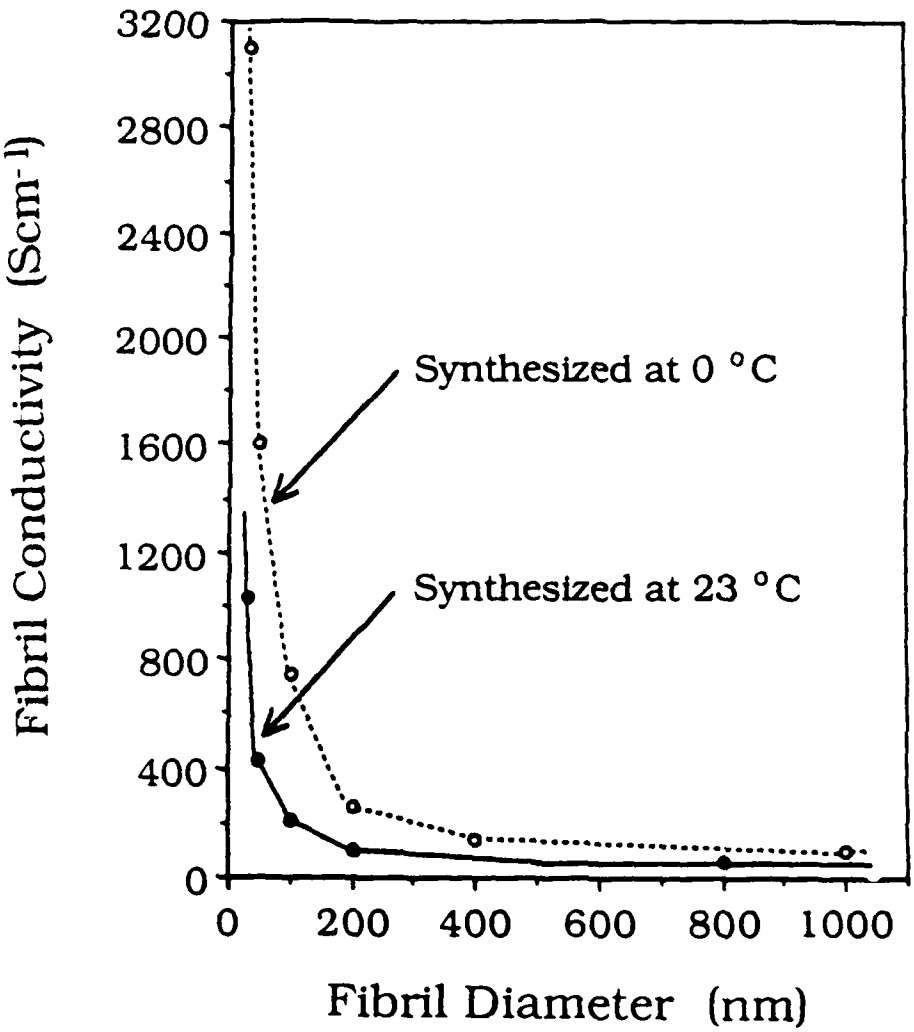
Fibril Conductivity (Scm-1)
3200
2800
2400
2000
1600
1200
800
400
0
0
200
400
600
800
1000
Fibril Diameter (nm)
Synthesized at 0 °C
Synthesized at 23 °C

Fig.

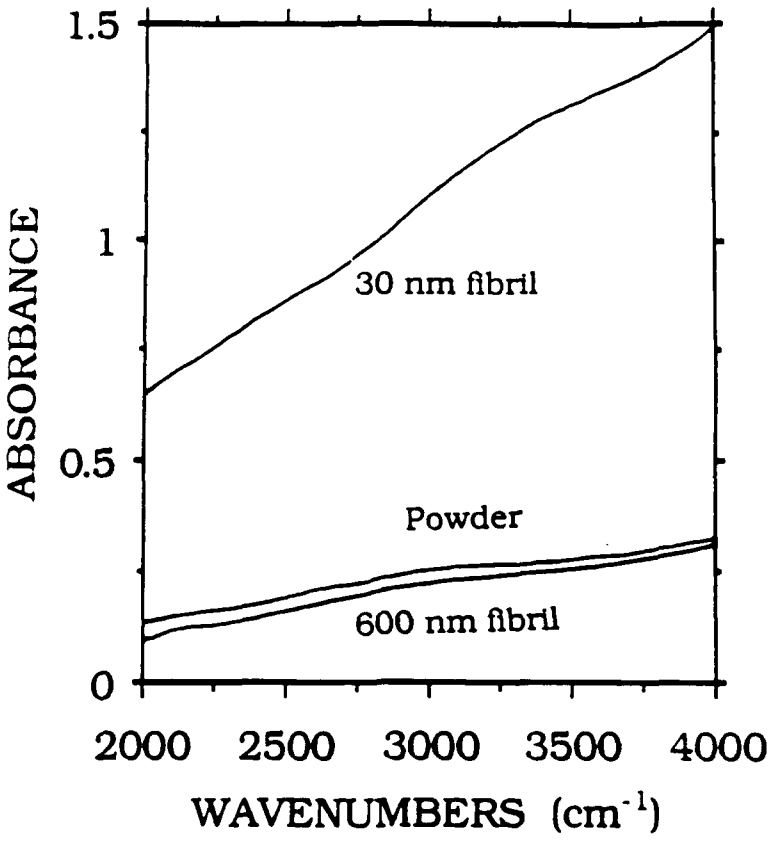
1.5
1
0.5
0
ABSORBANCE
30 nm fibril
Powder
600 nm fibril
2000
2500
3000
3500
4000
WAVENUMBERS (cm-1)

Fig. 8

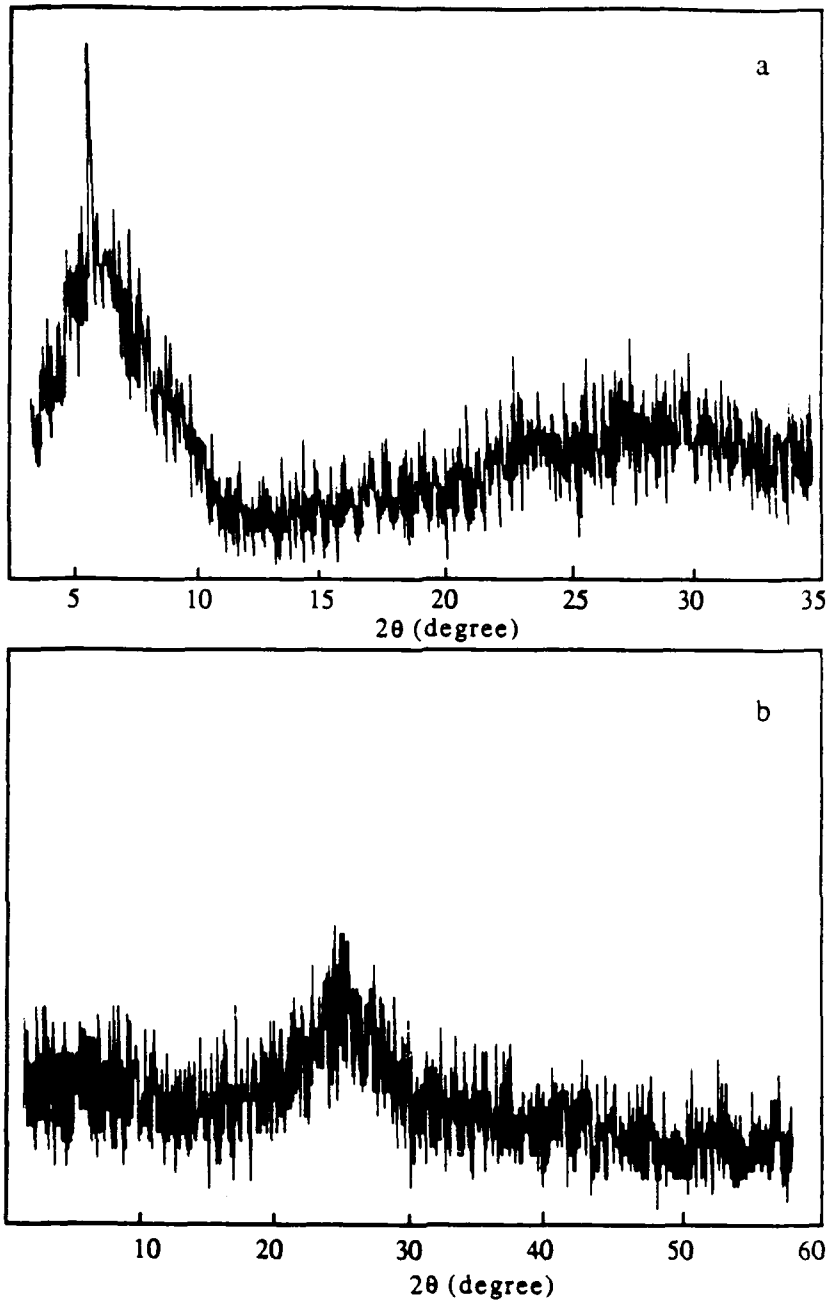


Fig. 9

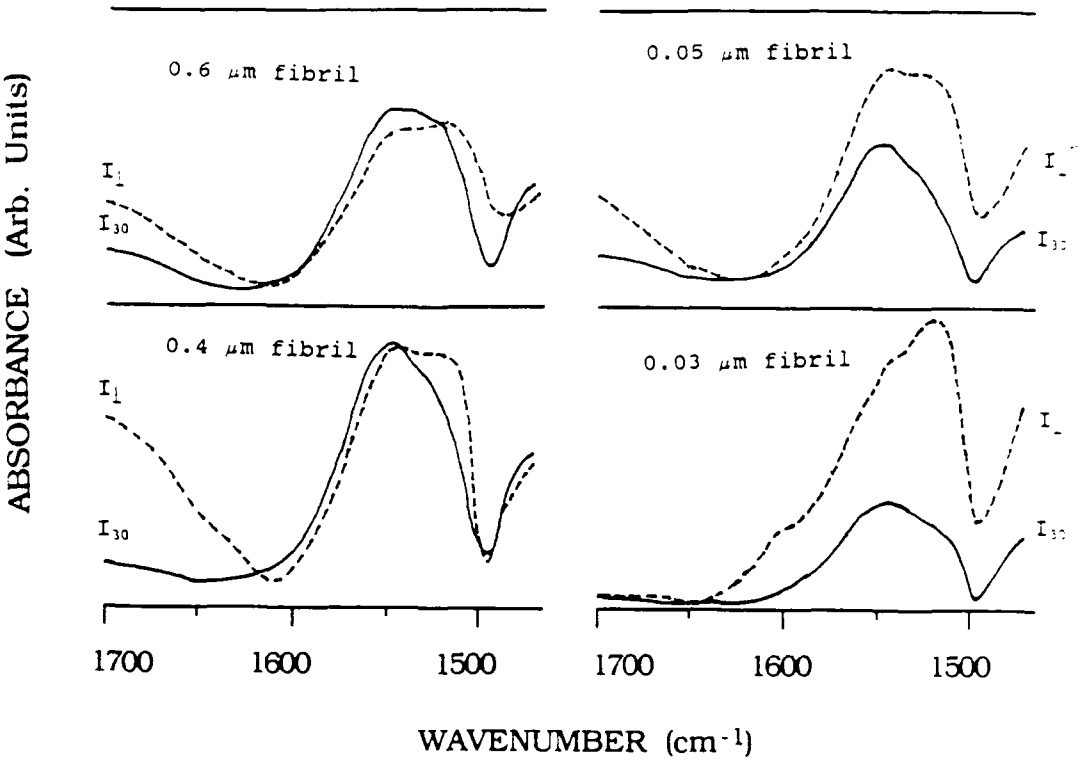
0.6 μm fibril
0.05 μm fibril
0.4 μm fibril
0.03 μm fibril
I⊥
I30
I∥
1700
1600
1500
ABSORBANCE (Arb. Units)
WAVENUMBER (cm-1)

Fig. 10

APPENDIX A - Effect of the surface layers.

We first show that the PPY surface layer does not contribute to the measured resistance across the fibril/Nuclepore composite. The conductivity of the PPY surface layer covering a fibril/Nuclepore composite membrane (30 nm-dia. pores) was measured using the standard four point method. A surface layer conductivity ($\sigma_s$) of 17 S $cm^{-1}$ was obtained. (This conductivity was based on a surface layer thickness of 200 nm.) The resistance across the surface layer ($R_s$) can be calculated via

$$R_s = d_s/(\sigma_s A_{Pt}) \qquad A1$$

where $d_s$ is the surface layer thickness (200 nm), and $A_{Pt}$ is the area of the upper Pt electrode (0.002 $cm^2$). An $R_s$ value of $6x10^{-4}$ Ω is obtained. This is less than 1 % of the smallest experimental membrane resistance shown in Table II. Thus, the surface layers do not contribute to the resistance measured across the fibril/Nuclepore composite.

We next show that we are justified in using the area of the upper Pt disk electrode to calculate the fibril conductivity. Note first that the area of the Pt electrode is significantly smaller than the area of the lower Ag particle electrode (Figure 1). It is, therefore, in principle possible that the "real" measurement area (i.e. the area in the membrane through which current flows during the resistance measurement) is larger than the area of the upper Pt disk. We will show below that this is not the case for the composite membranes investigated here.

Consider the diagram shown in Figure A1. By assuming that the Pt disk electrode area (defined by the radius of the Pt

electrode, $r_{pt}$ = 0.025 cm) is the relevant measurement area, we are, in essence, assuming that all of the current flows in the cylinder defined by the dashed lines in Figure A1. In fact, this will always be true when the radius of the electrode (0.025 cm) is much greater than the thickness of the film (10$\mu$). This is particularly true for the composite membranes investigated here.

Consider a hypothetical current line which flows outside of the cylinder defined by the area of the Pt disk electrode. This current must pass laterally along the PPY surface layer (this resistance is defined as $R_1$ in Figure A1), through the fibril/Nuclepore composite (resistance $R_2$ in Figure A1), and then through the lower PPY surface layer ($R_3$). The total resistance experienced by this current line then is $R_t = R_1 + R_2 + R_3$. We will consider only the resistance $R_1$ and we will show that this resistance is much larger than the experimental membrane resistances (Table II), indicating that the current through the hypothetical path in Figure A1 is negligibly small.

Obviously $R_1$ will increase linearly with the lateral distance the current travels through the PPY surface layer. We will begin by assuming that this distance is very small so as to minimize $R_1$ and thus maximize the probability that this current path will contribute to the total measured current. Let us assume that the length of the current path associated with $R_1$ is 0.00125 cm; i.e. we are assuming that $r_{ex}$ in Figure A1 is 0.02625 cm. This would make the radius associated with the "real" measurement area 5% larger than the radius of the Pt disk electrode ($r_{pt}$ = 0.025 cm). The resistance $R_1$ (Figure A1), can

then be approximated by (units are shown in parenthesis)

$$R_1 = \frac{0.00125\ (cm)}{17\ (\Omega^{-1}\ cm^{-1})\ 2\pi 0.02625\ (cm)\ 2\times10^{-5}\ (cm)} = 22\ \Omega$$

This $R_1$ is over 50 times larger than the largest measured membrane resistance (Table II). This indicates that negligible current flows through the path indicated in Figure A1.

One could lower $R_1$ by making the lateral current path in Figure A1 smaller. However, this would make $r_{ex}$ approximately equal to $r_{pt}$ (Figure A1) and thus the "real" measurement area would be the area of the Pt disk.

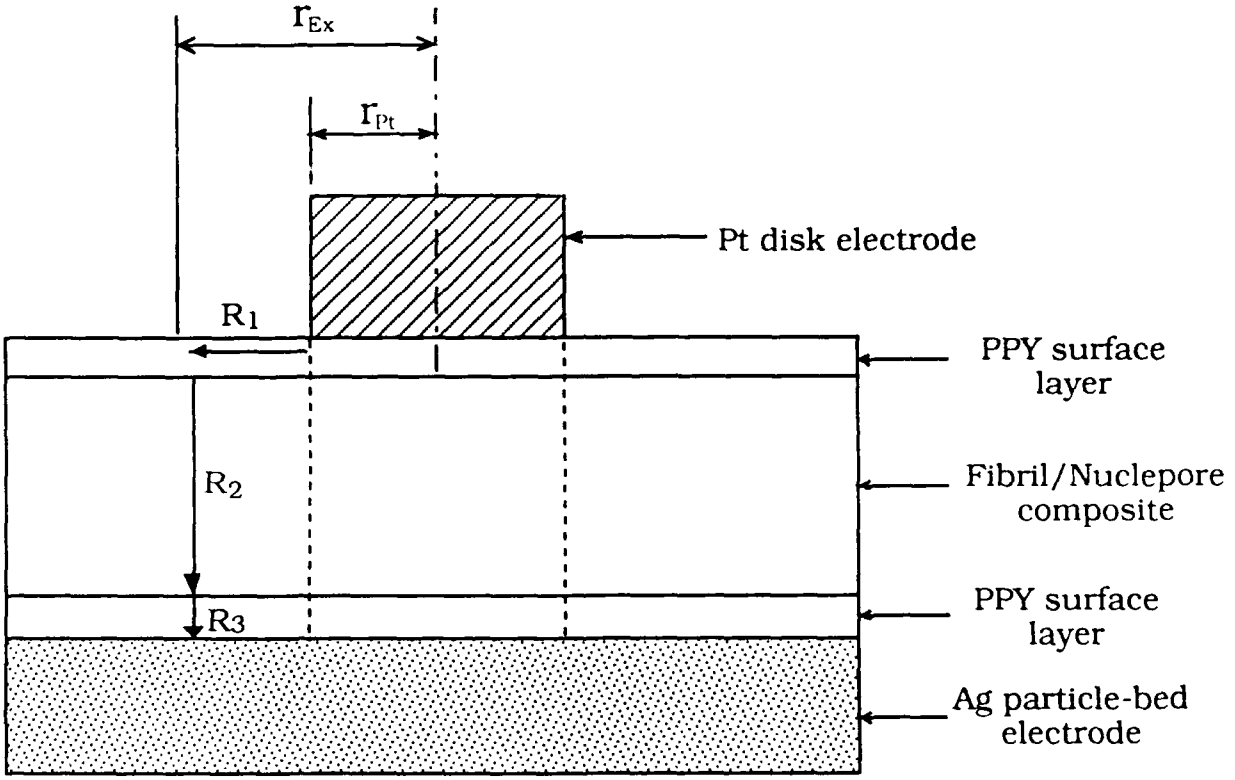
$r_{Ex}$
$r_{Pt}$
Pt disk electrode
$R_1$
PPY surface layer
$R_2$
Fibril/Nuclepore composite
$R_3$
PPY surface layer
Ag particle-bed electrode

APPENDIX B. Calculation of the fibril conductivity.

The apparatus shown in Figure 1 provides the bulk resistance of the composite membrane, $R_m$, which is given by

$$1/R_m = 1/R_f + 1/R_p \qquad (1B)$$

where $R_f$ is the parallel sum of the resistances of the conductive polymer fibrils and $R_p$ is the resistance of the intervening template membrane. Resistance measurements on virgin Nuclepore membranes show that $R_p >> R_f$ (). Thus, Equation 1 becomes

$$1/R_m = 1/R_f = n/R_i \qquad (2B)$$

where n is the number of fibrils in the measurement area and $R_i$ is the resistance of an individual fibril.

The number of fibrils in the measurement area can be obtained from the data in Table I and the known area of the Pt disk electrode. Thus $R_i$ can be calculated from $R_m$ (Equation 2B). $R_i$ and the area (A) and length (l) of the fibril (Table I) can be used to calculate the fibril conductivity ($\sigma_{fib}$)

$$\sigma_{fib} = l/R_i\ A \qquad (3B).$$

The above analysis assumes that conductive polymer grows only in the pores and not within the bulk polymer. To test this assumption, we attempted to grow polypyrrole within nonporous polycarbonate sheet. No evidence for PPY growth within the nonporous sheet was obtained and the resistance of these sheets remained essentially infinite.